Standardization of high-energy laser impact tests with respect to temperature, reflection and perforation time

OPEN ACCESS
IOP Publishing
Measurement Science and Technology
Meas. Sci. Technol. **36** (2025) 036008 (11pp)
https://doi.org/10.1088/1361-6501/adb171

Standardization of high-energy laser impact tests with respect to temperature, reflection and perforation time

J Wolfrum[1], R Schmitt[2], M Neuland[3], S Backfisch[3], J Speiser[4], B Weiss[5], S Kossenjans[6] and S Reich[7,*]

[1] Bundeswehr Research Institute for Materials, Fules and Lubricants (WIWeB), Institutsweg 1, 85435 Erding, Germany
[2] French-German Research Institute of Saint-Louis (ISL), 5 rue du Général Cassagnou, 68300 Saint-Louis, France
[3] German Aerospace Center (DLR), Institute of Technical Physics, Im Langen Grund, 74239 Hardthausen am Kocher, Germany
[4] German Aerospace Center (DLR), Institute of Technical Physics, Pfaffenwaldring 38-40, 70569 Stuttgart, Germany
[5] Federal Office of Bundeswehr Equipment, Information Technology and In-Service Support (BAAINBw), Ferdinand-Sauerbruch-Str. 1, 56073 Koblenz, Germany
[6] Bundeswehr Technical Center for Weapons and Ammunition (WTD 91), Schiessplatz, 49716 Meppen, Germany
[7] Fraunhofer Institute for High-Speed Dynamics, Ernst-Mach-Institut, EMI, Ernst-Zermelo-Straße 4, 79104 Freiburg, Germany

E-mail: stefan.reich@emi.fraunhofer.de

Received 1 October 2024, revised 15 January 2025
Accepted for publication 3 February 2025
Published 19 February 2025

Abstract

High-energy laser impact tests on identical materials and irradiation parameters often show deviating results between different testing institutes. This particularly affects the specular component of the reflection and the temperatures. Even the supposedly easy-to-determine perforation time sometimes shows large variations between different test institutes. For a reliable and reproducible determination of test results, a standardization of the experimental setups is necessary. Test results using two different reference materials are presented. These tests demonstrate that standardizing experimental setups and evaluation methods significantly reduces the deviations of the experimental results. The presented multi-institutional approach aims at gaining data of laser reflection, temperature, and perforation time of laser impacted samples, and at developing an optimized experimental setup based on different existing laboratory equipment and experimental approaches.

* Author to whom any correspondence should be addressed.

Keywords: high-energy laser, laser perforation, laser penetration, temperature measurement, specular reflection

1. Introduction

Lasers delivering high average powers are of increasing interest for defense applications [1, 2]. First demonstrator systems have been realized. By combination of several lasers (spectrally or coherently), output powers of up to 300 kW are realized up to now [1].

In addition to laser technology development, the laser-matter interaction at the target of interest must be studied to gain knowledge of the irradiation parameters required to achieve specific results. Different institutes have reported on laser penetration tests [3–14]. However, the direct comparability of the experimental results is not always given. Many parameters such as laser power, laser spot size, beam profile, beam divergence, sample material but also sample surface quality play important roles in the laser-matter interaction.

In preliminary investigations, as part of a national study, high-energy laser impact tests were carried out by industry partners and research institutes. The effect of high-energy laser radiation on various target materials and the resulting reflections were investigated. The first tests, carried out on identical materials, often showed deviating results between different testing facilities due to differences in laser parameters and measurement setup used in the experiments. Above all, this concerned the specular part of the reflection and the temperatures. But also, the supposedly easy-to-determine perforation time of the sample partly showed deviations between different testing facilities.

Within the scope of the working group 'AG Beschussversuche', initiated by the Federal Office of Bundeswehr Equipment, Information Technology and In-Service Support (BAAINBw), standards for carrying out high-energy laser impact tests and measurement methods for quantifying the effect on the target materials and laser light reflection were developed. For this purpose, almost identical high-energy laser impact test setups have been established at three research institutes over the past few years.

1.1. Effect of high-energy laser radiation on materials

Regarding the response of different materials subjected to high-energy continuous wave lasers, the knowledge base is limited, as these data are often classified and not published. In principle, various effects are to be expected when a material is exposed to high-energy laser radiation. This includes:

- Material removal through melting and vaporization: For this purpose, sufficient energy per volume must be coupled into the material, according to the heat capacity, enthalpy of fusion and enthalpy of vaporization. Heat conduction processes in the material as well as cooling are loss processes to be considered [5, 14–17].
- The exposure of a material to increased temperatures can result in a number of adverse effects, including changes in mechanical properties, the initiation of chemical processes (such as oxidation), and ultimately, a loss of functionality (e.g. strength) [10, 18]. This can even happen before material removal occurs.
- Heat conduction through an enveloping material can result in the heating of interior structures, functional elements, or energetic materials situated below the irradiated material layer. As a result, the deeper layers can be exposed to such high temperatures that their properties change, which can be detrimental. The critical temperature for such effects can be reached without a complete penetration of the top material layer. Experiments and modeling of such effects are discussed e.g. in [19–22].

The amount of energy coupled into the material per volume is an important variable for the laser matter interaction [14, 15, 17]. The same applies to the amount of heat coupled in per time and area, as it is the important driver for heat conduction processes or cooling. A very early description can be found in [23].

Laser material processing of metal components is a well-established industrial process. It has been addressed by experimental and modeling research during the last decades. The basics are covered in a large number of textbooks, e.g. [24]. Spot sizes of less than 1 mm in diameter are typically used for these processes. The power densities are typically well over 200 kW cm^{-2}. For even smaller spot diameters of less than 100 µm (compare e.g. [25]), intensities easily rise above 6000 kW cm^{-2}. Therefore, results from laser material processing are mostly inapplicable for the research on laser-material interaction with large spot sizes as described in this work.

The amount of published data on the effect of high-energy laser radiation with spot sizes in the centimeter range is small compared to the established laser processing. For laser weapon applications typical parameters (i.e. power $>$10 kW and spot sizes $>$1 cm^2), the number of publications is even smaller [8, 13, 14]. This shows that sufficiently powerful laser sources are still not widely available. Investigations are mostly performed in the range of 2 to 10 kW. A transfer of the results from low to high laser powers is possible to some extent. For example, scaling laws which allow for an extrapolation towards higher power are reported in [14].

An important aspect for a widely valid extrapolation is that the thickness of the sample is small compared to the spot size, preferably smaller. Furthermore, the irradiation times considered should be short, preferably shorter than the thermal

diffusion time. A good estimate of reasonable exposure times can be obtained from the thermal diffusion length D [23]:

$$D = 2\sqrt{\kappa \Delta t} = 2\sqrt{\frac{\lambda_{\text{th}}}{C\rho}\Delta t} \tag{1}$$

where κ is the thermal diffusivity, λ_{th} the thermal conductivity, C the heat capacity and ρ the density of the material. For aluminum alloys, κ typically is in the range of 90–100 $\text{mm}^2\,\text{s}^{-1}$ and for steel 4 to 20 $\text{mm}^2\,\text{s}^{-1}$. For a typical dimension of the spot (e.g. approximately 10 mm), this gives reasonable irradiation times of a few seconds.

Applying an air flow to the material surface during laser irradiation leads to further effects [3, 5, 6, 12, 16, 26]. Four different effects are to be expected, with their characteristics depending on the material, the coupled power density and the strength of the air flow. These are (i) cooling of the surface, (ii) forced ejection of molten material, (iii) removal of vapor, smoke, and possibly plasma in front of the sample and (iv) influence of occurring chemical processes.

The behavior of polymers differs from that of metals when exposed to high-energy lasers due to their physical and chemical properties. In metals, the light is absorbed within the first nanometers of depth. The absorption in plastics is much more dependent on the wavelength of the laser [27] and on the specific material. For example, poly(methyl 2-methylpropenoate) (PMMA) has a low level of absorption in the near infrared (IR) range. This primary limits heating and impact effectiveness. However, once the PMMA is heated up and has generated small bubbles, the directed transmission strongly drops and the scattering increases. This can distribute the radiation outside the primary irradiated area [11]. Besides the different absorption behavior, the thermal properties are also different. Typically, polymers have a low thermal conductivity. Therefore, heat is not efficiently dissipated and therefore, a localized rapid heating occurs in the event of high-energy laser impact. Also, several physical and chemical changes can occur in the material as a result of this heating process. Thermoplastics such as polycarbonate or polyethylene may be subject to melting and vaporization. In contrast, thermosetting polymers such as epoxy or phenolic resins will usually undergo chemical degradation and carbonization prior to sublimation [28, 29]. These changes also have an effect on the optical and mechanical properties of the material, e.g. absorption can be increased by carbonization [30], whereas mechanical strength is reduced [18, 31].

1.2. Perforation time as a measure of sample failure

The accurate determination of the exact perforation times for the different materials is important for the description and modeling of the lethality of different targets. This is an assessment of the probability of survival and the development of possible protective materials that can withstand high-energy laser radiation over a certain period of time. These results can be also used to validate numerical simulation methods [15] and to develop relatively simple 'Engineering'-Models for a fast assessment of the potential damage caused by high energy weapon lasers [10].

In [3, 32] the excellent protective behavior in terms of a high perforation time of aluminum is described. This behavior is explained in terms of rapid heat conduction along the axial direction. Paint, depending on the paint properties, can increase or decrease the perforation times [6]. Regardless of laser power and spot size, the thicker the material, the longer the drilling time [32].

Reich *et al* showed recently that at high laser powers reaching 100 kW, the perforation times of aluminum are no longer greater compared to steel [14]. For spot diameters of $D4\sigma =$ 35 mm and a sample thickness of 10 mm at around 80 kW, equal perforation times are observed while above this laser power, the aluminum samples get perforated first.

1.3. Characterization of the reflection

Laser reflections may pose a threat to third parties. Therefore, these possible health risks during free field usage must be quantified. The reflections from the target materials can evoke Nominal Ocular Hazard Distances (NOHD) amounting from meters up to several kilometers, depending on the material properties and laser parameters [13, 33, 34]. This can cause permanent eye and skin damage, as well as injury to operators [33]. Moreover, high-power light intensities scattered towards the equipment or ammunitions on-board the platform hosting the laser can also be dangerous and compromise the safety and integrity of the platform itself. In [33] a methodology is proposed for the calculation of NOHD for high-energy lasers.

It was shown that the reflectance decreases dramatically at elevated temperatures [35]. This was addressed to changes in the surface properties of the metals and composite materials investigated. The surfaces discolored. A large reflectance transition was observed for the polished and plated steel plates. The experiments also showed that the polished aluminum alloys had a higher and the composite materials a lower overall reflectance compared to the polished and plated steel plates.

Laser light reflecting from a target material is composed of two main components. The first is a specular reflected component. It is a mirror-like reflection and exists when the surface is smooth with a roughness smaller than the wavelength. The second component comes into play when surfaces have a larger roughness. Then they show a significant contribution of diffuse reflection. On the small scale, a mirror-like reflection of the single surface facets might still exist. However, since these facets are not aligned to each other, the angle of mirror-like reflection is not homogeneous. Therefore, the diffuse reflected light has a certain angular distribution with components in up to all direction. An ideal diffuse reflection surface follows the Lambert's cosine law. Macro-scale regularities such as production related parallel grooves can lead to distinct diffuse scattering distributions. This can roughly be regarded as a widening of the laser beam.

Experiments to assess the complex reflection behavior of metallic samples irradiated by high-energy lasers were performed e.g. in [13, 33, 34, 36]. The experiments characterized the reflected power in a narrow central field of view and the spatial and temporal distribution of the reflection patterns. A modeling of the reflected beam separated the reflections into three components: a specular, a forward scattered and a Lambertian component [34]. The latter both are diffuse reflections which follow different models. The Lambertian contribution results in a uniform scattered intensity distribution following the Lambert's cosine law. The NOHD values are small. Under the assumption of a 30 kW-laser, only some meters were estimated [34]. The forward scattered contribution was defined as the part of the reflection which follows the ABg-model [37]. The NOHD distances for the forward scattering estimated in [34] were found to be roughly two orders of magnitude larger than the Lambertian values. Note that the ratios are material dependent.

The specular component, which is a mirror-like reflection, leads to the largest NOHD. It can exceed several kilometers. Considering a 30 kW-laser and worst-case assumptions regarding divergence, reflected power, sample curvature and atmospheric attenuation, Henrichsen *et al* [34] found NOHD values for tinplate samples of 14.3 km for the specular contribution. These worst-case NOHD values were valid only for a very short time after the start of the irradiation. The experiments shown in this work show that the radiant power values decrease over the irradiation time—one can, therefore, expect decreasing NOHD values.

2. Experimental

2.1. Experimental setup

All three institutes involved are using the same kind of experimental setup as a matter of principle. A well-defined laser beam of power P_{nom} 0.5, 1.5 and 5.0 kW and diameter $D4\sigma = 10$ mm hits the target of interest. Part of the laser power is absorbed by the sample leading to heating, melting and maybe evaporation. This is strongly dependent on the sample material and also the applied laser power. The other part of the radiation is reflected specularly and diffusely (see definitions in the introduction). Finally, the target gets penetrated by the laser due to material melting and flow-out or evaporation until the radiation is partly or fully transmitted.

A schematic of the experimental setup is shown in figure 1. More details on the specific configurations of the three different setups are listed in table 1.

The individual institutes use different lasers for the experiments. However, it is anticipated that the slight deviation of the laser wavelength λ does not have a major impact on the results. For the final laser beam hitting the sample, a spot diameter of $D4\sigma = 10$ mm (evaluated by ISO 11 146-1:2005 [38]) and a divergence of less than 1 mrad was settled. The beam divergence was guaranteed for at least a few tens of centimeters, which is much larger than the sample thickness. The spot size can therefore be considered constant for these experiments. As

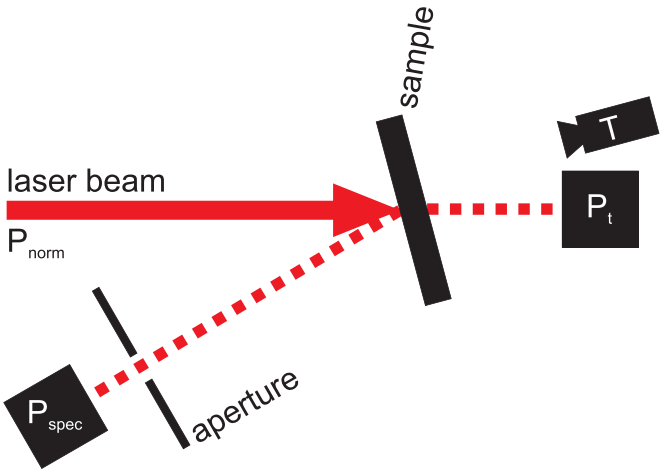

Figure 1. Schematic of this principle of the experimental setup. The laser beam with defined power P_{norm} hits the sample. The mirror-like reflected power P_{spec} is measured as power in the bucket of defined aperture. The backside temperature T is detected with infrared techniques. After sample perforation, the transmitted power P_{t} is detected.

the experiments were conducted in laboratories, any effects of beam disturbance on propagation in the atmosphere, such as turbulence or thermal blooming, were excluded and would have been beyond the scope of this paper.

The radiation reflected and scattered on the sample is expected to have at least two components. Part of the radiation is reflected under the mirror angle without increasing the divergence. This part is called specular reflection within this paper. Some of the radiation is reflected diffusely or scattered with a significant increase of the divergence, thus we will call it the diffuse reflection in the following.

Due to the nature of the experiments, it is not possible to clearly distinguish specular and diffuse reflection. Therefore, the differentiation between specular and diffuse reflection was realized by using the principle of the power-in-the-bucket. An aperture to measure the radiation reflected in specular direction (P_{spec}) was defined to be 15 mm in diameter in 1 m distance from the sample located at the mirror angle. For the measurement of the specular reflection, a fast power meter (Institutes 1 and 2) or an integrating sphere with a fast photodiode (Institute 3), both with a corresponding mechanical aperture, were used.

The power P_{t} transmitted through the sample was used as the criterion for the sample perforation time. P_{t} was measured indirectly by photo diodes oriented on the beam dump (Institutes 1 and 2) or a water cooled integrating sphere (Institute 3). A defined ratio $P_{\mathrm{t}}/P_{\mathrm{nom}}$ could be used as a trigger signal for stopping the laser emission, and also for determining the perforation time of the sample. The perforation time and the time for stopping the laser emission do not have to be equivalent.

During the experiment, the backside temperature of the samples was measured. All institutes used IR cameras, which always requires the knowledge of the emissivity of the

Table 1. Details on the sensors and techniques applied in the three equivalent setups of the three institutes.

	Institute 1	Institute 2	Institute 3
Laser	Trumpf TruDisk 6001 (4 C) $P = 180$–6 kW $\lambda = 1030$ nm $M^2 \approx 20$	IPG YLS-10 000 $P = 60$–10 kW $\lambda = 1070$ nm $M^2 \approx 16$	IPG YLS-10 000 $P = 60$–10 kW $\lambda = 1070$ nm $M^2 \approx 16$
Specular reflex	Coherent Power Max-Pro 3 kW	Coherent Power Max-Pro 3 kW	integrating sphere with photo diodes
Measurement of transmitted power	photo diode (PDA10CS InGaAs) power calibrated	photo diode Not calibrated	integrating sphere (water-cooled) with photo diode, power calibrated
Backside temperature	InfraTec Variocam HD 0 to 2000 °C 7.5 to 14 µm	FLIR A655sc 7.5 to 14 µm, 50 Hz, 14 bit two-color pyrometer SensorTherm M322: 600 °C to 2300 °C, H322: 400 °C to 1200 °C Both 1.65 to 1.8 µm and 1.45 to 1.65 µm	FLIR A655sc Telops HDR M350: 3.0 to 5.4 µm 2x pyrometer LumaSense Inc. IMPAC IN5H+, IMAPC IN5/5+ Both 8 to 14 µm
Video surveillance	2× Axis camera, V59 series	2× Basler ace-series	4× Axis camera, Basler ace-series

observed spot for determining the absolute temperatures. Since large changes in the temperature and thus phase changes of the materials occurred in these experiments, the temperature dependent emissivity would have been required but is not available. Furthermore, the pristine emissivity of bar aluminum is very low [39]. Therefore, these samples were painted with thermal resistant paints on the back side (at Institutes 2 and 3). The other samples were used as delivered. The temperature determined was, by definition, the temperature for an emissivity of 0.95. In first approximation this is a reasonable value for all bare used samples as well as the thermal resistant paints (data not shown here). The area used for temperature reading was around 0.5 mm^2 large and was located in the center of the laser spot.

Institutes 2 and 3 additionally used pyrometers to derive sample temperatures at the same spot as derived from the IR images. The two-color pyrometers of Institute 2 have spot sizes of about 1 mm and have the advantage that they are independent of the emissivity, assuming a constant emissivity within the two neighboring channels. However, the minimum measurable temperature was limited to 400 °C. The pyrometers of Institute 3 (spot size around 6 mm) required the emissivity to be adjusted. Therefore, the same points have to be considered as for the IR cameras.

In addition, videography in the optical wavelength range of the sample front- and backside were recorded with different cameras. As the initial purpose of these videos was for optical observation rather than quantitative analysis, no specific requirements were specified. Nonetheless, optical images can provide valuable insights into discrepancies observed during measurements, particularly in circumstances involving diffuse scattered radiation or sample penetration.

The various instrument signals were captured either by the manufacturer's software or by data acquisition units with the appropriate sampling rate and bit depth. The timing of all instruments and lasers was done by master signals with referencing for each instrument.

2.2. Materials

All investigations were performed on two different commercially available materials:

- Polished aluminum samples with average roughness of Ra = 0.1 µm according to DIN EN ISO 21 920-2 [40] and a dimension of 100 × 100 × 10 mm^3. At Institutes 2 and 3, the backs of the samples were painted with heat-resistant paint. This was done to better determine the temperature using IR radiation based pyrometers and IR cameras.
- Extruded black dyed polyamide 6 (PA6) samples with a dimension of 100 × 100 × 5 mm^3 (TK Hennecke GmbH, Germany).

All sample material was ordered centrally at one time and then delivered to the three institutes. Therefore, there can be no batch-to-batch variation due to different production of the same material. All institutes had exactly the same samples.

3. Results and discussion

The aim of this work is the validation of equivalent experiments performed at different institutes with at least partly different equipment. Therefore, the main focus of the presented results is on the comparability of the experimental results and not on the exact retrieved values.

3.1. Perforation times

The perforation times were determined based on the onset of significant transmission through the sample. Figure 2 presents

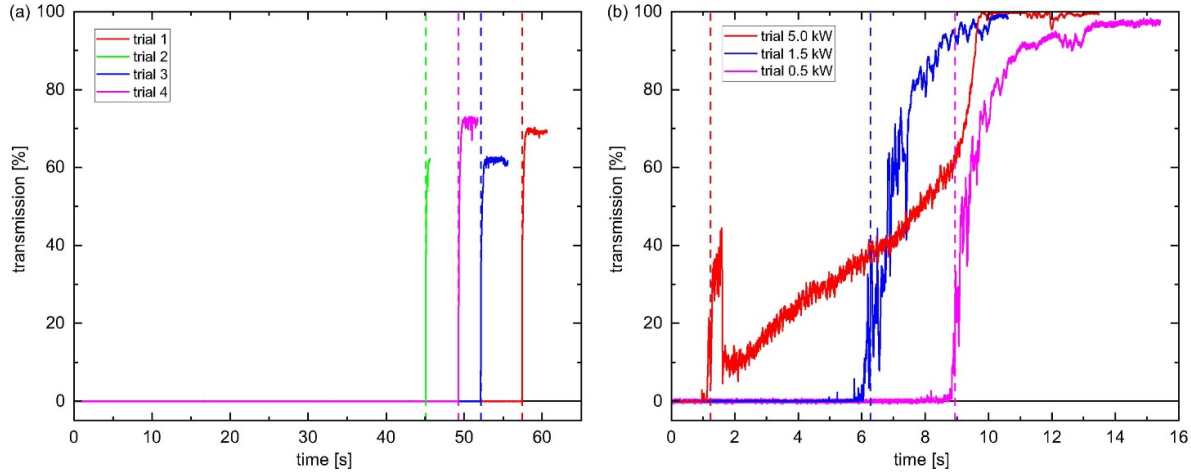

Figure 2. Curves of laser power transmission through the samples of selected experiments. As illustrated in (a), the transmission of four identical experiments of aluminum samples irradiated with a laser power of 5.0 kW demonstrates a well-detectable perforation and a substantial variance in perforation time. In (b) a worse detectable perforation time for black dyed PA6 samples can be seen for the three laser powers of 0.5, 1.5 and 5.0 kW. The vertical dashed lines represent the extracted perforation times.

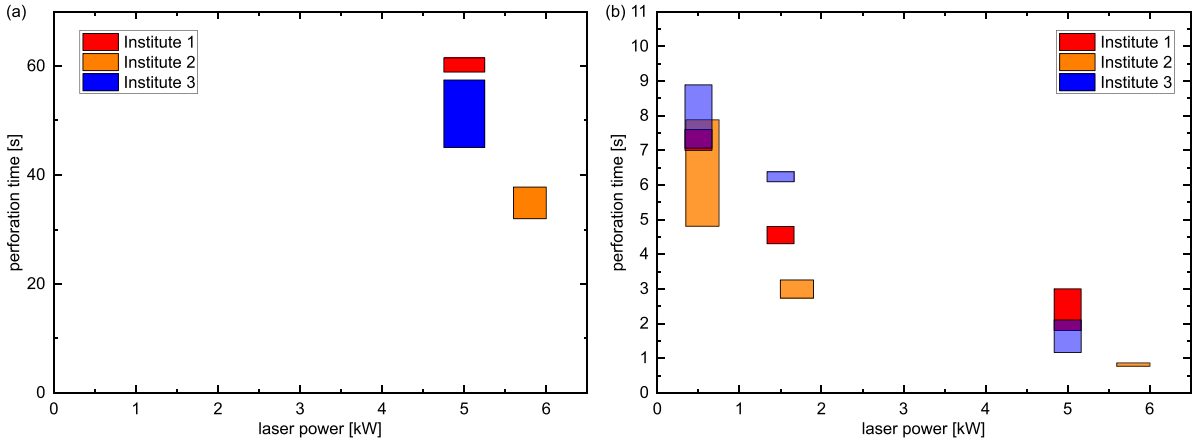

Figure 3. Perforation times (range of observed values) for the aluminum (a) and PA6 black dyed (b) samples. For aluminum, a perforation was observed only for a laser power of 5 kW. For the black dyed PA6 samples, a decreasing perforation times with increasing laser power is observed.

exemplary transmission curves for both investigated materials. Aluminum was perforated only for the highest laser powers used. In figure 2(a), the transmission curve for four identical experiments with aluminum samples at one institute for a laser power of 5.0 kW is shown. It is observed that the perforation times vary from 45 to 57.5 s, with an average of 50.1 s for this particular institute. The determination of perforation times can be made with a high degree of clarity, given the rapid increase in signal intensity to values above 50%.

In figure 2(b) the three transmission curves of the laser detection sensor for the PA6 samples irradiated with 0.5, 1.5 and 5.0 kW are shown. It can be seen that the actual perforation times cannot be evaluated as clearly as for the aluminum samples. This is due to the fact that the melt film of PA6 ruptures briefly but closes again, at least partially, before the real final perforation takes place. This effect leads to short peaks in the diagram just before the final perforation of the material. Sometimes, as shown here for the experiment with 5.0 kW, even large holes with high transmission are formed, which then shrink and reduce the transmitted power before reopening. For the determination of the perforation time, only the final perforation of the material was evaluated.

Figure 3(a) shows the perforation times for the aluminum samples for a laser power of 5.0 kW. At 0.5 and 1.5 kW, no perforation was achieved within the maximum irradiation time used. The heating of the samples was too slow to exceed the melting temperature of aluminum (see discussion on backside temperature in the next section). Institute 2 had a slightly higher laser power at the target. The significant smaller perforation times, however, are not completely explainable with that. On the other hand, also for Institute 1 and 3 the perforation times do not overlap with each other. At all institutes the same processes were observed. The aluminum samples melt in the area of laser irradiation, form a molten bubble (see therefore also [41]) and then suddenly the melt flows out. The perforation time can clearly be determined due to the significant signal

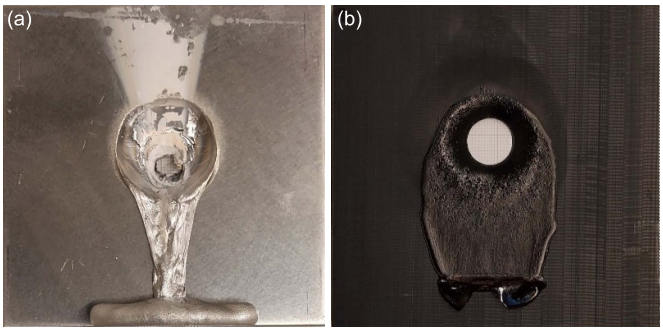

Figure 4. Front side images after perforation with a laser power of 5.0 kW of the samples made of (a) Al and (b) black dyed PA6. Sample sizes are 100 × 100 mm^2.

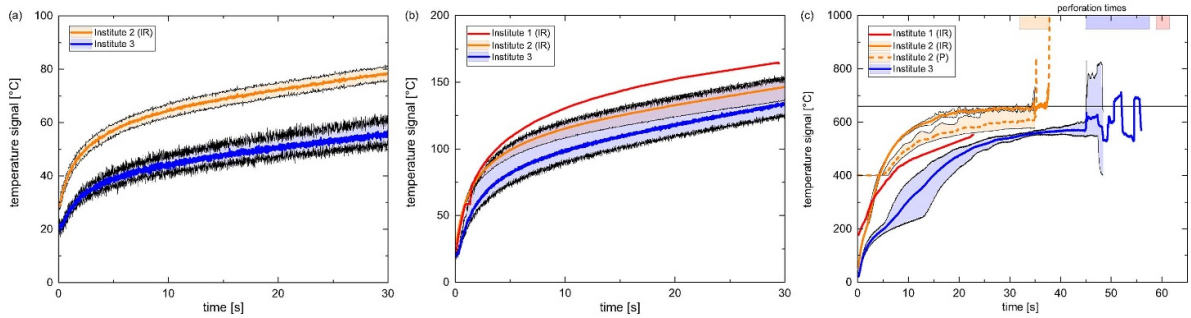

Figure 5. Backside temperatures of the polished aluminum samples as a function of time for the three different laser powers 0.5 kW in (a), 1.5 kW in (b) and 5.0 kW in (c) measured with IR-camera (IR) and/or with pyrometer (P).

increase (see figure 2(a)). However, the melt dynamics leads to a high variance of the time point of the flow-out of the material. Due to this complex penetration and melt through process this leads to significant changes in the perforation times and a high variance. Overall, a poor reproducibility was expected and observed.

In figure 3(b) the perforation times for black dyed PA6 material are presented. The perforation times show similar values for the three different institutes. It is noteworthy that Institute 2 has again determined the shortest perforation times. The strongest deviations are found for 1.5 kW.

Figure 4 shows exemplary front side images of the samples after perforation for a laser power of 5.0 kW. For the aluminum samples (figure 4(a)), the molten aluminum has flown out of the heat affected zone. The hole is almost constant in size throughout the sample thickness. Only a thin layer mostly at the back side of the sample has remained. This was observed at all institutes. The origin is not fully clarified. In figure 4(a) a hole in the sample of about the size of the laser spot is observable. The heat affected zone is centered above the laser spot location (flow-out area compared to hole in the sample). This was also observed by Reich *et al* [41] at least for spot sizes similar in size. A further investigation of the underlying process of this incomplete flow-out of the molten material is beyond the scope of this work. Above the hole, a white powder deposit can be observed. This originates from oxidation processes during the laser impact and consists of oxidized material components from the aluminum alloy.

The front side of a perforated black dyed PA6 panel is shown in figure 4(b). The emerged hole has a conical shape. It is almost rotationally symmetric. Since PA6 is a thermoplast, part of the sample flows out. In contrast to the aluminum sample, it is spread more to the sides. This implies a different flow-out process. Furthermore, an even larger heat affected zone can be observed with roughly double the size of the final hole.

3.2. *Backside temperatures*

All institutes measured the backside temperatures with IR-cameras (IR) and/or with pyrometers (P). Figure 5 shows the backside temperatures of the polished aluminum samples as a function of the time for the three different laser powers. Note, there is no valid temperature data for Institute 1 and 0.5 kW. As expected, it is evident from the data that higher laser powers correspond to increased temperatures, including maximum temperatures. For laser powers of 0.5 kW and 1.5 kW, there is good agreement in the observed temperature increases over time among the different institutes. For the laser power of 5.0 kW, larger deviations in the temperature courses between the different institutes can be observed. On the one hand, Institute 3 observed overall lower temperatures compared to the other two institutes. Even at the perforation time, values much below the melting temperature of aluminum (horizontal black line in figure 5(c)) were observed.

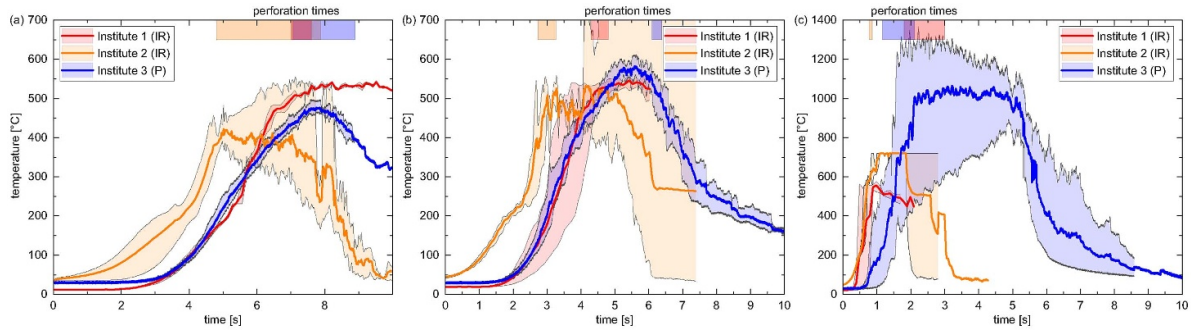

Figure 6. Backside temperatures of the black dyed PA6 samples as a function of time for the three different laser powers 0.5 kW in (a), 1.5 kW in (b) and 5.0 kW in (c) measured with IR-camera (IR) and/or with pyrometer (P). The solid line represents the mean value, while the shaded areas correspond to the minimum and maximum value range. At the top of each graph, the range of observed perforation times are indicated.

This data was recorded with a pyrometer, for which the knowledge of the emissivity is required. Therefore, a not perfectly matched emissivity value can lead to such underestimated temperature values. At Institute 2, the temperature progression was measured both by IR-camera and pyrometer. It should be noted that the two-color pyrometer only can record temperature data above 400 °C. In principle, the temperature curves of the IR-camera and the pyrometer show reasonable agreement beyond 400 °C. The slight offset in the temperatures of approximately 50 °C between the IR-camera and the pyrometer might originate from the different wavelength regions and sampling sizes of date extraction.

At 5 kW, the temperatures first saturate near the melting temperature of aluminum at about 660 °C. Until the perforation, no higher temperatures are observed. Aluminum has got a high thermal conductivity and furthermore shows a certain convective flow within the melt pool, which causes a spread of the introduced energy over even a larger area than the laser spot size. Directly at the perforation time, the detected temperature rises very fast to significantly higher values than the melting point. The origin is not elucidated in more detail but most likely originates from a further heating of the molten material. These temperature jumps are observed at all institutes. However, they deviate strongly between the institutes and also show a high variance between single experiments at each single institute. Any temperature values after the perforation can not be regarded as valid values since the emergence of the temperature signal is unclear.

Figure 6 illustrates the temperature increase of the backside temperatures of the black dyed PA6 samples as a function of time for the three different laser powers. Analogous to the previous measurements on the aluminum samples, a steeper temperature increase with increasing laser power can be observed. For the laser powers of 0.5 kW and 1.5 kW, the temperature courses and the maximum temperatures agree relatively well. For the laser power of 5.0 kW, only the rate of the temperature increases agrees well, but the onset of the increases does not coincide. Optical observation shows that significant amounts of smoke are produced on both sides of the samples. This smoke can lead to a decrease of laser power hitting the sample which reduces the temperature increase. Furthermore, also the temperature measurement can be disturbed if smoke is within the line of sight. Then maybe the temperature of the smoke is detected rather than the sample temperature.

It is noteworthy that for all three laser powers, the maximum temperature considerably exceeds the melting temperature T_M of PA6 ($T_M \approx 225$ °C to 235 °C). Molten material as well as decomposition products and outgassing products can reach much higher temperatures than the melting temperature. The very high temperatures observed by Institute 3 and 5.0 kW originate very likely from hot vapor.

3.3. Specular reflected intensity

Figure 7 shows the specular reflected intensity of the polished aluminum samples as a function of time for the three different laser powers. At a laser power of 0.5 kW a small decline of the specular intensity can be observed within the first seconds. This effect is less pronounced at Institute 3. Thereafter, a constant level for the specular reflected intensity can be observed for all three institutes. Institute 2 and 3 observe values of around 20% of the irradiated power while Institute 1 observed higher values of above 30%. At a laser power of 1.5 kW, at the Institutes 1 and 2, a stronger decline of the specular intensity within the first seconds is again observed. Institute 3 recorded significant lower values right at the beginning. Thereafter, the specular intensity flattens out at a level of approximately 5% of the irradiated intensity. At 5.0 kW, all institutes observed an immediate steep decline in the specular intensity at the beginning of laser irradiation. For Institute 1 and 2, the intensity goes down to almost zero within the first two seconds. For Institute 3, a slightly slower decline of the reflection can be observed.

The specular reflected intensities of the black dyed PA6 samples are almost not measurable for all three laser powers. The measured values are low (<0.5 % of the irradiated power), which is within the detection limit of the laser detection sensors of Institute 1 and 2. Only Institute 3 could detect such low intensities.

Despite some differences in the absolute values and the exact temporal development, a good agreement between the

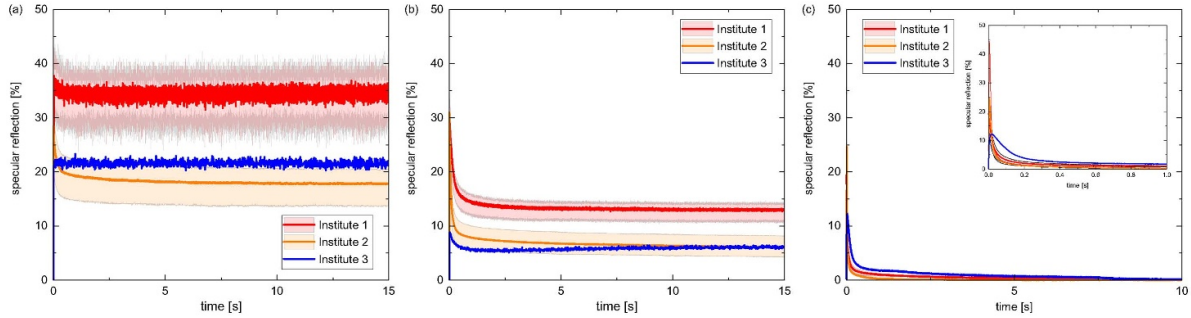

Figure 7. Relative specular reflected power of the polished aluminum samples as a function of time for the three different laser powers 0.5 kW in (a), 1.5 kW in (b) and 5.0 kW in (c). The colored line is the average and the light colored area around represents the range of measured values. For the two lower laser powers, all institutes measured in accordance a slight decrease within the first seconds and a saturation afterwards. For the 5.0 kW, measurement a comparable behavior was measured again but with a much faster decrease to much lower values.

three institutes was reached. At least within the measurement range of the different used devices, no significant differences can be observed. The cooled integrating sphere used at Institute 3 has the advantage of a higher dynamic range, especially suitable for low intensities.

4. Conclusions

The aim of this experimental study was to achieve uniform and reliable results for laser impact tests conducted with equivalent setups at three different research institutes. The first step towards this goal was the standardization of the test setup and measurement techniques between the different institutes. To compare the results, laser impact tests with two different commercially available reference materials were carried out. Therefore, samples of the materials have been exposed to continuous-wave laser radiation with three different powers while maintaining the laser spot diameter constant for all experiments. To compare the results, the perforation times, the back side temperatures and the specular part of the reflected intensity were evaluated.

The results for the perforation times showed a relatively good agreement between the institutes. The perforation times of aluminum samples showed larger differences between the institutes compared to the black dyed PA6 samples. This is consistent with the overall higher variance observed in the aluminum samples. It was shown that for aluminum samples, the perforation with a significant transmission of laser light through a sample hole happens within milliseconds and therefore the determination of the proper perforation time is easy. For the black dyed PA6 however, the transmitted power increases only within seconds. This required a stricter definition of how the perforation time is determined.

The backside temperature can be measured with different measurement devices. Depending on their measurement principle and sample emissivity, a painting with thermal resistant color can improve IR measurements which require the knowledge of the sample emissivity. Overall, a good agreement between the different institutes was observed with respect to variance within each institute. An increase of the maximum temperatures as well as a steeper increase in temperature with increasing laser power can be observed. It is noteworthy that for the black dyed PA6 material, the maximum temperatures consistently considerably exceeded the melting temperature. This is probably due to decomposition of the polymer and/or an subsequent heating of the melt during the laser irradiation.

For the polished aluminum samples, the specular reflected intensity shows a decline within the first seconds for all laser powers. Only minor differences between the institutes in the temporal course of the specular reflected power was observed. This showed again that different measurement principles, fast power meters or integrating spheres lead to comparable results. After this primary decline, a constant level for the specular reflected intensity is observable for laser powers of 0.5 and 1.5 kW. At a laser power of 5.0 kW, all institutes characterized an immediate steep decline in the specular intensity at the beginning with an almost vanishing intensity after the first seconds. A slight discrepancy was noted in the rate of decline between Institute 1 and 2 in comparison to Institute 3. The underlying cause of this discrepancy, namely whether it is attributable to the use of a different device by Institute 3, remains uncertain. For the black dyed PA6 samples, the specular reflected intensities are very low. For Institute 1 and 2, they are within the measurement limit and therefore undetectable. Institute 3 with a more sensitive device could measure specular reflected intensities. The observed values are within the noise level of the devices of the other institutes.

Overall, it was demonstrated that with properly defined setups at three different institutes it is possible to gain comparable data for high-energy laser impact tests. However, precise specifications of the experimental setup including laser parameters and measurement techniques must be made and adhered to. For a comparison of results in literature, all these definitions normally must be given to be able to compare the results. Only with such well defined experiments experimental results are exchangeable between institutes.

Data availability statement

The data that support the findings of this study are available upon reasonable request from the authors.

Acknowledgments

We acknowledge financial support by the Federal Office of BAAINBw, Germany.

Conflict of interest

The authors declare that they have no known competing financial interests or personal relationships that could have appeared to influence the work reported in this paper.

ORCID iDs

R Schmitt https://orcid.org/0000-0001-9385-5013
S Backfisch https://orcid.org/0009-0006-4780-3371
S Reich https://orcid.org/0000-0002-8405-6540

References

[1] Karr T and Trebes J 2024 The new laser weapons *Phys. Today* **77** 32–38
[2] Venugopal V 2024 Zapping enemy targets: viable laser weapons remain critical to military strategy photonics focus
[3] Boley C, Fochs S and Rubenchik A 2008 Large-spot material interactions with a high-power solid-state laser beam *J. Dir. Energy* **3** 15–24
[4] Boley C D, Cutter K P, Fochs S N, Pax P H, Rotter M D, Rubenchik A M and Yamamoto R M 2010 Interaction of a high-power laser beam with metal sheets *J. Appl. Phys.* **107** 043106
[5] Baek W, Lee K, An S, Shin W and Yoh J 2013 Melt-through characteristics in continuous beam irradiation of flying metal samples in flow speeds up to 85 m/s *Opt. Laser Technol.* **45** 250–5
[6] Baumann S M, Hurst B E, Marciniak M A and Perram G P 2014 Fiber laser heating and penetration of aluminum in shear flow *Opt. Eng.* **53** 122510
[7] Khairallah S A, Anderson A, Rubenchik A M, Florando J, Wu S and Lowdermilk H 2015 Simulation of the main physical processes in remote laser penetration with large laser spot size *AIP Adv.* **5** 047120
[8] Schleijpen R H A, Binsbergen S V, Geljon M, Meuken D, Deiana D and van Leeuwen B 2020 30kw laser experiments against drones *Technologies for Optical Countermeasures XVII; and High-Power Lasers: Technology and Systems, Platforms, Effects IV* ed D H Titterton, R J Grasso, M A Richardson, W L Bohn and H Ackermann (SPIE) (https://doi.org/10.1117/12.2574461)
[9] Hustedt M, Niedens V, Brodeßer A, Bauche T, Hermsdorf J and Kaierle S 2021 Assessment of steel shields for protection against laser radiation *J. Laser Appl.* **33** 042053
[10] Wolfrum J, Eibl S, Oeltjen E, Osterholz J and Wickert M 2021 High-energy laser effects on carbon fiber reinforced polymer composites with a focus on perforation time *J. Compos. Mater.* **55** 2249–62
[11] Schmitt R, Meyer T, Pätzold R, Kokot J and Fischer B 2022 Experimental investigations on the response of metallic and dielectric materials to laser irradiation in the kW range *Procedia CIRP* **111** 859–63
[12] Schäffer S, Allofs D, Gruhn P, Gülhan A, Lueck M and Osterholz J 2022 *Experimental Investigation of High-Power Laser Irradiation of Missile Materials in Subsonic and Supersonic Flows High-Power Lasers and Technologies for Optical Countermeasures* ed D H Titterton, R J Grasso, M A Richardson, H Ackermann and W L Bohn (SPIE) (https://doi.org/10.1117/12.2647841)
[13] Meuken D, Binsbergen S A V, Scheers L, van den Berg P and van Eijk A M J 2022 *Reflection Measurements in TNO's 30 kW Laser Facility High-Power Lasers and Technologies for Optical Countermeasures* ed D H Titterton, R J Grasso, M A Richardson, H Ackermann and W L Bohn (SPIE) (https://doi.org/10.1117/12.2634047)
[14] Reich S, Goesmann M, Heunoske D, Schäffer S, Lueck M, Wickert M and Osterholz J 2023 Change of dominant material properties in laser perforation process with high-energy lasers up to 120 kilowatt *Sci. Rep.* **13** 21611
[15] Horak J, Heunoske D, Lueck M, Osterholz J and Wickert M 2015 Numerical modeling and characterization of the laser-matter interaction during high-power continuous wave laser perforation of thin metal plates *J. Laser Appl.* **27** S28003
[16] Wei C, Zhu Y, Zhou M, Ma Z and Wu T 2017 Melt removal mechanism by transverse gas flow during laser irradiation *4th Int. Symp. on Laser Interaction With Matter* ed Y Ding, G Feng, D H H Hoffmann, J Cao and Y Lu (SPIE) (https://doi.org/10.1117/12.2267060)
[17] Osterholz J, Heunoske D, Horak J, Lexow B, Lueck M, Schaeffer S and Wickert M 2017 Experimental characterization of energy transfer from large-diameter kilowatt continuous-wave laser beams to metal samples *J. Laser Appl.* **29** 012011
[18] Allheily V, Merlat L and Hostis G-L 2019 *Experimental and Numerical Investigations of Laser-Induced Thermal Effects on Composite Materials High Power Lasers: Technology and Systems, Platforms, Effects III* ed D H Titterton, H Ackermann and W L Bohn (SPIE) (https://doi.org/10.1117/12.2532258)
[19] Osterholz J, Lueck M, Lexow B and Wickert M 2016 *Neutralization of Improvised Explosive Devices by High-Power Lasers: Research Results From the FP7 Project Encounter High-Power Lasers 2016: Technology and Systems* ed H Ackermann, W L Bohn and D H Titterton (SPIE) (https://doi.org/10.1117/12.2241083)
[20] Garcia J D, Joyce P and Brownell C 2016 Thermal damage behind HEL-irradiated carbon fiber-reinforced polymer skin *J. Dir. Energy* **6** 119–36
[21] Schmitt R and Allheily V 2018 Modelling the heating process of CFRP by cw-laser radiation with special focus on the heat transfer by thermal radiation between the carbon fibers *Procedia CIRP* **74** 562–7
[22] Schmitt R 2019 Modelling of the thermal initiation process for encased explosives *High Power Lasers: Technology and Systems, Platforms, Effects III* ed D H Titterton, H Ackermann and W L Bohn (SPIE) (https://doi.org/10.1117/12.2532554)
[23] Schriempf J T 1974 Response of materials to laser radiation: a short course *Technical Report* Naval Research Laboratory
[24] Steen W M and Mazumder J 2010 *Laser Material Processing* (Springer) (https://doi.org/10.1007/978-1-84996-062-5)
[25] Wetzig A, Baumann R, Herwig P, Siebert R and Beyer E 2015 Laser remote cutting of metallic materials: opportunities and limitations *Industrial Laser Applications Symp. (Ilas 2015)* vol 9657, ed M Green and C Rose (SPIE) p 965708
[26] Boley C and Rubenchik A 2008 Modeling of laser-induced metal combustion *Technical Report* Lawrence Livermore National Lab.(LLNL)
[27] Chen M, Zak G and Bates P J 2015 Absorption coefficient measurement in laser transmission welding of thermoplastics *Int. Polym. Process.* **30** 38–43
[28] Bras M L, Rose N, Bourbigot S, Henry Y and Delobel R 1996 The degradation front model- a tool for the chemical study

of the degradation of epoxy resins in fire *J. Fire Sci.* **14** 199–234
[29] Torre L, Kenny J M and Maffezzoli A M 1998 Degradation behaviour of a composite material for thermal protection systems Part I–Experimental characterization *J. Mater. Sci.* **33** 3137–43
[30] Schmitt R and Allheily V 2023 *Modelling the Heating of Gfrp by High-Energy Laser Radiation Considering the Pyrolysis of Binder Material Technologies for Optical Countermeasures XIX* ed R J eGrasso, M Eichhorn and G D Lewis (SPIE) (https://doi.org/10.1117/12.2678922)
[31] Hilado C J 1998 *Flammability Handbook for Plastics* (CRC Press) (https://doi.org/10.1201/9780585248684)
[32] Taillandier M, Peiffer R, Colomer B, Ortiz R, Chalumeau E and Pommies M 2022 *High-Energy Laser Experiments for Vulnerability Studies in the Context of the European Talos Program High-Power Lasers and Technologies for Optical Countermeasures* ed D H Titterton, R J Grasso, M A Richardson, H Ackermann and W L Bohn (SPIE) (https://doi.org/10.1117/12.2635076)
[33] Daigle J F, Pudo D, Théberge F and Châteauneuf M 2017 Laser safety evaluation for high-energy laser interaction with solids *Opt. Eng.* **56** 026106
[34] Henrichsen M, Schwarz B, Ritt G, Azarian A and Eberle B 2021 Laser safety assessments supported by analyses of reflections from metallic targets irradiated by high-power laser light *Appl. Opt* **60** F71
[35] Freeman R K, Rigby F A and Morley N 2000 Temperature-dependent reflectance of plated metals and composite materials under laser irradiation *J. Thermophys. Heat Transfer* **14** 305–12
[36] Bailey A, Early E, Kennedy P and Thomas R 2016 Automatic construction of probabilistic dynamic bidirectional reflectance distribution functions from reflection screen images *Reflection, Scattering and Diffraction From Surfaces* ed V L M Hanssen (SPIE) (https://doi.org/10.1117/12.2235343)
[37] Pfisterer R N 2011 Approximated scatter models for stray light analysis *Opt. Photon. News* **22** 16–17
[38] Deutsche Fassung EN ISO 11146-1:2005 2005 *DIN EN ISO 11146-1:2005-04, Laser und Laseranlagen - Prüfverfahren für Laserstrahlabmessungen, Divergenzwinkel und Beugungsmaßzahlen - Teil 1: Stigmatische und einfach astigmatische Strahlen (ISO 11146-1: 2005)* International Organisation for Standardization (https://doi.org/10.31030/9572886)
[39] Reynolds P M 1961 Spectral emissivity of 99.7 % aluminium between 200 and 540 °C *Br. J. Appl. Phys.* **12** 111–4
[40] Deutsche Fassung EN ISO 21920-2:2022 2022 *DIN EN ISO 21920-2 :2022-12, Geometrische Produktspezifikation (GPS) - Oberflächenbeschaffenheit: Profile - Teil 2: Begriffe und Kenngrößen für die Oberflächenbeschaffenheit (ISO 21920-2:2021, korrigierte Fassung 2022 -06)* (International Organisation for Standardization) (https://doi.org/10.31030/3294017)
[41] Reich S, Göbel A, Goesmann M, Heunoske D, Schäffer S, Lueck M, Wickert M and Osterholz J 2022 2D and 3D triangulation are suitable in situ measurement tools for high-power large spot laser penetration processes to visualize depressions and protrusions before perforating *Materials* **15** 3743